JOURNAL OF PROPULSION AND POWER
Vol. 24, No. 6, November–December 2008

Spray Characteristics of a Recessed Gas–Liquid Coaxial Swirl Injector

Li-jun Yang* and Ming-he Ge†
Beihang University, 100083 Beijing, People's Republic of China
Meng-zheng Zhang‡
Northwestern Polytechnical University, 710100 Xi'an, People's Republic of China
and
Qing-fei Fu§ and Guo-biao Cai¶
Beihang University, 100083 Beijing, People's Republic of China

DOI: 10.2514/1.23977

The effect of recess length on the internal flow development and spray characteristics of a gas–liquid-swirl coaxial injector was investigated both theoretically and experimentally. Three different flow patterns were identified and explored as a function of the recess length. The spray-field dynamics and droplet-size distribution were measured by means of a high-speed photographic technique. An improved theoretical model was established to correlate experimental observations. An expression of the optimal recess length for atomization was obtained.

Nomenclature

A	=	geometrical characteristic parameter of the swirl injector
ch	=	hyperbolic cosine function
d	=	spout diameter
e	=	2.7183
f	=	friction coefficient
H	=	recess length
L	=	length of the injector element
P_0	=	reverse pressure
$\bar{R}$	=	dimensionless radius of the vortex chamber
r_{bx}	=	radius of the tangential channel
r_m	=	radius of the gas vortex
S	=	dimensionless radius of the gas vortex, r_m/r_c
sh	=	hyperbolic sine function
V	=	liquid velocity
α, β	=	unknown coefficient
ΔP	=	pressure drop of the swirl injector
θ	=	spray-sheet cone angle
μ	=	mass flow discharge coefficient
ν	=	viscosity of liquid
π	=	3.141592
ϕ	=	recess angle
φ	=	flow area ratio, F_l/F_c

Subscripts

c	=	spout of the swirl injector
g	=	gas
k	=	vortex chamber
l	=	liquid
real	=	real value
T	=	theoretical value
test	=	tested value
ux	=	tangential partial quantity
xx	=	axial partial quantity

Superscripts

-	=	dimensionless parameter
′	=	pulsation component

Received 17 March 2006; revision received 7 July 2008; accepted for publication 7 July 2008.

*Associate Professor, School of Astronautics.
†Graduate Student, School of Astronautics.
‡Graduate Student.
§Ph.D. Student, School of Astronautics.
¶Professor, School of Astronautics.

I. Introduction

RECESSED shear coaxial injectors were first introduced during the development of the J-2 rocket engine in 1963. From then on, more efforts were made to study the effects of recess length on coaxial-injection characteristics and the ensuing influences on combustion efficiency and the stability of the thrust chamber. In spite of the vast amount of information obtained thus far, no conclusive results have been reached. According to the results of some investigations, the effect of the recess of the center injector on droplet sizes for the coaxial injector is not clear and can be neglected [1–3]. Sankar et al. [4] and Sasaki et al. [5] measured the spray characteristics of coaxial injectors by means of phase Doppler particle analysis, examining the effects of the recess length of the oxidizer center port on the sizes of liquid droplets, velocity, and mass flux. With increased recess length for the oxidizer center port, effects on liquid-droplet sizes developed. The investigation by Hannum et al. [6] found that the mean droplet size may decrease when the liquid-oxidant injector is recessed. Combustion efficiency will increase when the liquid-oxidizer center port is recessed. It can be deduced that improved atomization quality will improve combustion efficiency. According to Sankar et al. [7], if the recess distance is less than one-half of the diameter of the oxidizer center port, the mean size of the liquid droplets will increase, due to the recess of the oxidizer center port. Falk [8] claimed that based on a single measurement, the recess of the oxidizer center port has little effect on the mean droplet size. Gomi [9] observed that if there is no recess or the injector diameter is 3 times the recess distance, there is very little difference among liquid-droplet dimensions. Glogowski and Micci [10] modeled the design of their injector on the space shuttle's main engine. They focused on the velocity and droplet-size distribution immediately downstream of the liquid-injection port. They changed the geometry and recess of the liquid-injection port and measured the effect on the velocity and droplet-size distribution. Glogowski and Micci concluded that a tapered water-injection port reduced the velocities of the spray within the flame-stabilization region.

Glogowski et al. [11] also studied the instability mechanisms in a coaxial injector with a recessed region and no recessed region. Bazarov [12] investigated the theory that the liquid jet in the submerged region of the coaxial injector undergoes high-frequency oscillation and fluctuation during the jet-breakup process; he called these phenomena *self-oscillation* and *self-pulsation*. The pulsation frequency was presumed to correlate with the time required for the liquid to propagate through the recessed region. He also verified that the recess length of the injector is the most important parameter determining the self-pulsation characteristics. Kim and Heister [13] aimed at increasing understanding of the hydrodynamic instability inside the coaxial injector. They developed a 3-D incompressible unsteady viscous Navier–Stokes solver for the coaxial jet atomization in a recessed region of the injector. Their model incorporates the chamber pressure perturbation and also enables modeling the injection-coupled instability of the injector flow.

Experimental results suggest that the recess distance between the end faces of the oxidizer center port and the outer fuel injector has very important effects on the efficiency and stability of combustion; the mechanisms are currently under investigation. Many studies have explored the effect of the oxidizer center-port recess length on the spray characteristics of coaxial injectors based on the atomization in cold flow, but no consensus was reached. In this paper, the effect of recessing the oxidizer center port on the atomization characteristics of a coaxial swirl injector was investigated in detail, both theoretically and experimentally.

II. Theoretical Analysis

A. Analysis of Flow Models in the Recessed Mixing Chamber

When recess length is used as the characteristic parameter of a recessed mixing chamber [1], the flow conditions in the chamber are determined not only by the recess distance, but also by the diameters of the concentric inner liquid and outer gas flows of the coaxial injector. Recess distance is, however, inconvenient for mathematical analysis. Therefore, the concept of recess angle ϕ is proposed in this paper. Recess angle ϕ is used as the characteristic parameter so that the effect of the recess on the spray characteristics can be analyzed conveniently. Recess angle is defined in Eq. (1) and shown schematically in Fig. 1. If the recess length changes from 0 to ∞, the recess angle will change from π to 0. The recess angle is a linear function of the recess length, including the other geometric dimensions of the coaxial-injector exit, and so we can fully account for the effect of the recess on the flow characteristics in the recessed mixing chamber of the coaxial injector:

$$\phi = 2tg^{-1}[(d_g - d_l)/(2H)] \tag{1}$$

Comparing the recess angle with the spray angle of the liquid-swirl center port, the interaction of the outer gas flow and the inner liquid film in the mixing chamber for different recess lengths can be classified into three categories. If the recess angle is 180 deg, the recess distance will be zero, and the recessed mixing chamber will not exist. The interaction of the gas flow and the liquid film happens completely outside the coaxial-injector spout. This is called an outer mixing flow. The recess angle will decrease with an increase in recess length. When the recess angle decreases to nearly equal the spray angle (namely, $180 > \phi > \theta$), liquid film cannot impact the inner surface of the gas spout, and the gas-flow tube is not completely closed by liquid film. Excessive space between the inner liquid film in the swirl center port and the outer gas injector's inner surface means that the inside of the gas flow atomizes the liquid, and the outer gas flow spurts into the chamber without participating in atomization. In this case, the gas–liquid phase occupies a small part of the recessed mixing chamber, the gas phase occupies a large section, and the recessed mixing chamber has little effect on the gas–liquid interaction. The outer gas flow and inner swirl liquid film interact mainly outside the recessed mixing chamber, and the flow is

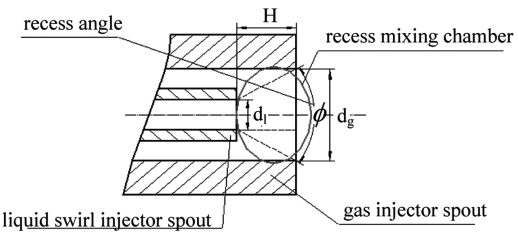

Fig. 1 Definition of recess angle for the coaxial swirl injector.

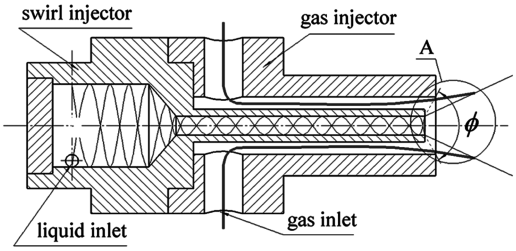

a) Injector configuration

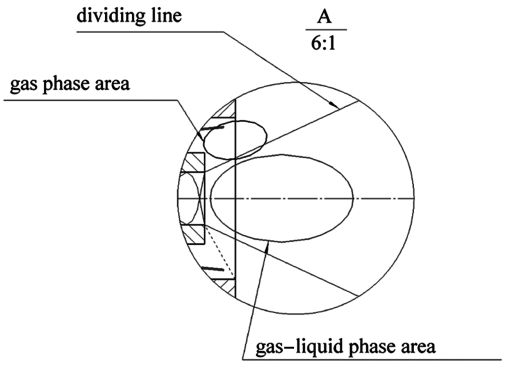

b) Outer mixing flow condition

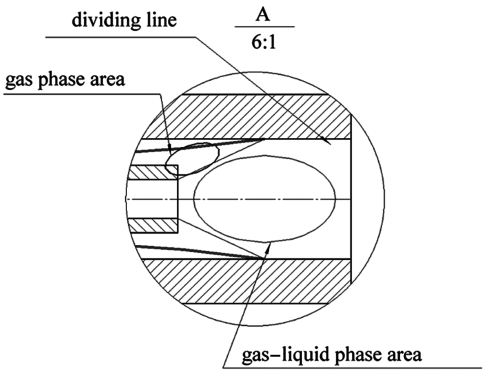

c) Inner mixing flow condition

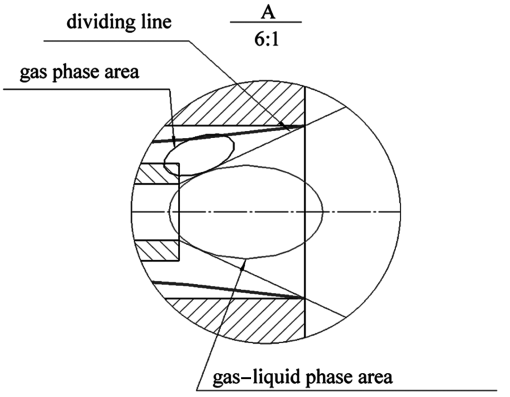

d) Critical recess flow condition

Fig. 2 Recessed-mixing-chamber configurations.

classified as an *outer mixing flow*. If the swirl liquid center port is recessed further so that the recess angle equals spray angle of the swirl center port (namely, $\phi = \theta$), the liquid film of the swirl center port will touch the rim of the outer gas concentric port. This is called a *critical recess*. In this condition, outer gas flow is completely closed by the inner swirl liquid film, and all of the gas flow impacts on the surface of the liquid film for atomization.

The recess angle will decrease as the inner swirl center port is recessed. If the recess angle is less than the spray angle of the inner swirl port (namely, $\phi < \theta$), the swirling liquid film will touch the inner surface of the outer gas port, and the gas–liquid-phase area will occupy a large section of the recessed mixing chamber. In this case, the outer gas flow and inner liquid film mainly interact in the recessed mixing chamber, and the flow is referred to as an *inner mixing flow*. The swirling liquid film will contact the inner surface of the outer gas injector so that both the gas flow and the inner surface of the outer port will act on the inner swirl liquid film and contribute to atomization. The effects on liquid atomization are quite complicated. The recess-angle configuration is shown in Fig. 2.

According to the preceding analysis, the flow conditions in the recessed mixing chamber are greatly influenced by the recess length, flow conditions of the gas–liquid-phase section, and different mechanisms of atomization. Among the three configurations presented, the gas–liquid mixing flow of the critical recess is the most favorable for atomization. This is because the entire gas flow acts on the atomization at the critical recess condition, compared with the other two configurations. To validate this hypothesis, experiments on a long-spout swirl injector and steady-atomization characteristics of a recessed coaxial swirl injector were performed.

B. Theoretical Calculation of the Spray-Sheet Cone Angle of the Swirl Injector

The thickness of the liquid film in the spout of the swirl injector is much less than the spout radius, and so the axial velocity V_{xx} and tangential velocity V_{ux} must be included in the calculation, but the radial velocity can be neglected [14]. In the axial direction, define a differential volume dm by coordinate value x, differential length dx, and thickness $r_c - r_m(x)$, shown in Fig. 3.

The following expressions can be deduced according to the basic theory of the swirl injector:

Geometrical characteristic parameter, including the spout length of the swirl injector:

$$A_T = \frac{A_{kT}}{\mathrm{ch}(f\bar{L}_c/4\varphi) + \mathrm{sh}(f\bar{L}_c/4\varphi)\sqrt{\varphi^2 A_{kT}^2 + 1}} \tag{2}$$

Spray-sheet cone angle:

$$tg\frac{\theta_T}{2} = \frac{\bar{V}_{ux}}{\bar{V}_{xx}} = \frac{[2\mu_T A_T/(1+S)]}{\sqrt{1-[2\mu_T A_T/(1+S)]^2}} = \frac{2\mu_T A_T}{\sqrt{(1+S)^2 - 4\mu_T^2 A_T^2}} \tag{3}$$

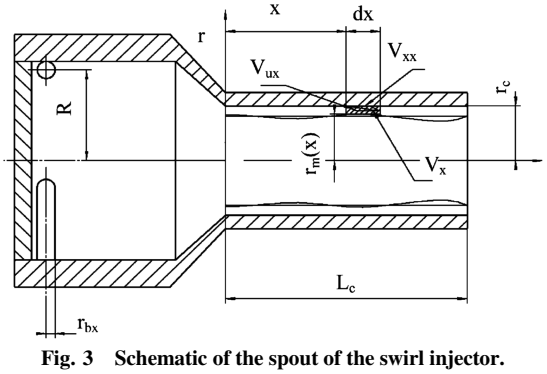

Fig. 3 Schematic of the spout of the swirl injector.

III. Experimental Setup and Procedures

The experimental system consists of a simulated propellant supply system, pressure and flow measurement system, and high-speed dynamic testing system (some typical testing results are shown in

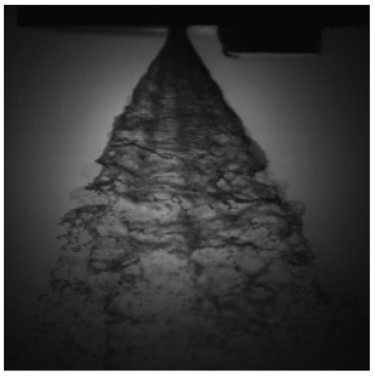

a) H=19.5 mm

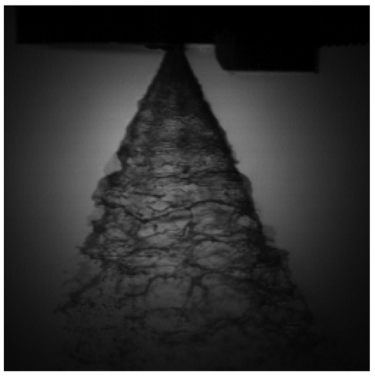

b) H=20.7 mm

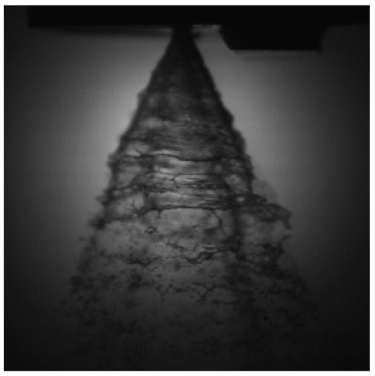

c) H=23.7 mm

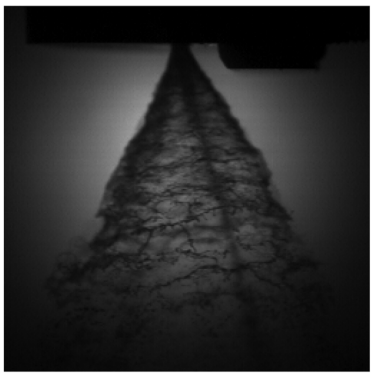

d) H=25.2 mm

Fig. 4 Photographs of the swirling jet for different swirl-injector spout lengths ($A = 4$ and $\Delta P = 0.65$ MPa).

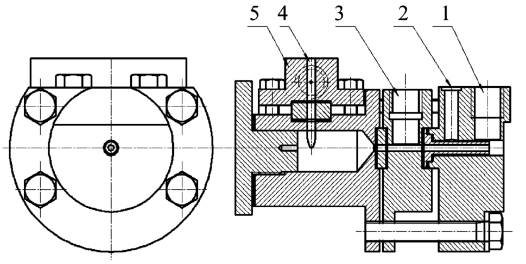

Fig. 5 Structure of the modal injector: recessed mixing-chamber pressure tap (1), air inlet (2), spout pressure tap (3), water inlet (4), and tangential passage pressure tap (5).

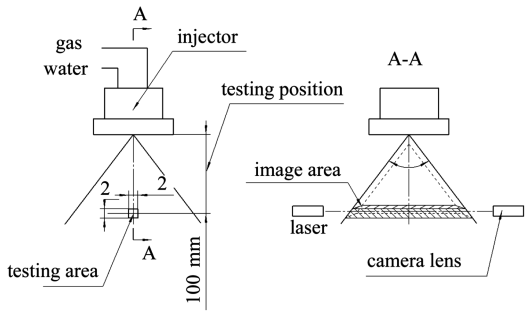

Fig. 6 Test area and test point position.

Fig. 4). Water and compressed air are used as the liquid and gaseous propellants, respectively. The common spray measurement devices (such as a Marvin laser-scattering size analyzer, phase Doppler particle analyzer, etc.) could only measure the steady spray field, and

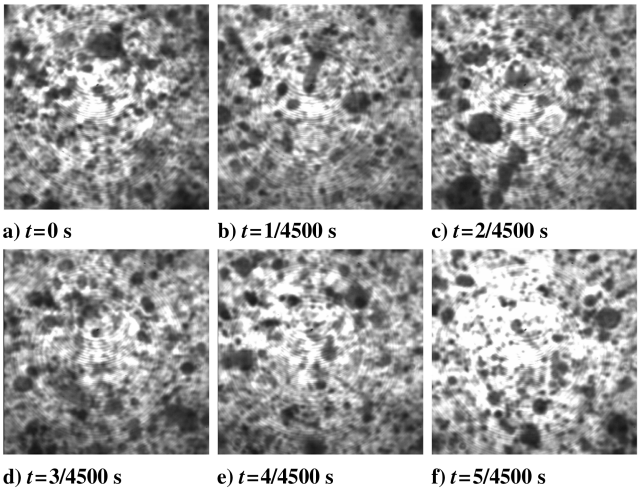

Fig. 7 Droplet photograph shot by high-speed camera.

they are not appropriate for dynamic spray-field measurement. The high-speed dynamic measurement system consists of copper-vapor laser light sheet illumination, Ultima-40K high-speed digital camera, control system, image analysis PC, and image analysis system. The system record and analysis of the spray process is at the frame rate of 4500 frames per second. This system has the temporal and dimensional statistics ability and can calculate the Sauter diameter, mass mean diameter, volume mean diameter of the droplets, droplet-size distribution, and speed of the droplet. The resolution of the testing system is no less than 40 μm, with a measurement tolerance of less than 10%. The system was calibrated using standard particleboard.

Table 1 Comparison of spray-sheet cone angles: theoretical vs experimental

$\bar{R}$	$\bar{f}$	A_{kT}	φ	S	$\bar{L}_c$	A_T	$f\bar{L}_c/4\varphi$	θ_T	θ_{test}
					0.6	1.9125	0.0095	79.8	73.02
					19.5	1.3039	0.3096	65.8	49.98
2	0.03175	1.938	0.5	0.7874	20.7	1.2747	0.3286	64.8	50.49
					23.7	1.2053	0.3762	62.7	47.05
					25.2	1.1723	0.4001	61.6	59.48
					0.6	3.2834	0.0131	91.3	72.87
					19.5	1.8720	0.4266	68.2	64.76
4	0.0322	3.352	0.3680	0.8567	20.7	1.8137	0.4528	66.8	50.58
					23.7	1.6777	0.5184	62.9	53.45
					25.2	1.6144	0.5513	61.7	54.57
					0.6	3.7347	0.0187	90.6	88.40
					19.5	1.7639	0.6082	56.7	56.54
6	0.0375	3.842	0.3006	0.8869	20.7	1.6911	0.6456	54.8	53.63
					23.7	1.5243	0.7391	50.5	56.18
					25.2	1.4481	0.7859	48.3	57.54

Table 2 Sizes of experimental coaxial injectors

Type of coaxial injector	Recess distance, mm	Radius of gas spout r_c, mm	Radius of liquid spout r_c, mm	Liquid spout length L_c, mm	$A = (r_c R/nr_{bx}^2)$	Type of the swirl injector
TZ-8-20.85	5.7	2.3	1.0	19.5	2	LX-8-7.35
TZ-8-22.12	4.5	2.3	1.0	20.7	2	LX-8-9.25
TZ-8-23.56	3.0	2.3	1.0	22.1	2	LX-8-10.5
TZ-8-25.1	1.5	2.3	1.0	23.7	2	LX-8-11.4
TZ-8-26.63	0	2.3	1.0	25.2	2	LX-8-13.25
TZ-12-20.85	5.7	2.3	1.0	19.5	4	LX-12-7.35
TZ-12-22.12	4.5	2.3	1.0	20.7	4	LX-12-9.25
TZ-12-23.56	3.0	2.3	1.0	22.1	4	LX-12-10.5
TZ-12-25.1	1.5	2.3	1.0	23.7	4	LX-12-11.4
TZ-12-23.56	0	2.3	1.0	25.2	4	LX-12-13.25
TZ-16-20.85	5.7	2.3	1.0	19.5	6	LX-16-7.35
TZ-16-22.12	4.5	2.3	1.0	20.7	6	LX-16-9.25
TZ-16-23.56	3.0	2.3	1.0	22.1	6	LX-16-10.5
TZ-16-25.1	1.5	2.3	1.0	23.7	6	LX-16-11.4
TZ-16-23.56	0	2.3	1.0	25.2	6	LX-16-13.25

Table 3 Comparing recess angles of the smallest SMD and liquid sheet angle

Pressure drop of the liquid-swirl injector, MPa	Geometric characteristics of swirl injector A								
	2			4			6		
	ϕ, deg	θ, deg	θ–ϕ, deg	ϕ, deg	θ, deg	θ–ϕ, deg	ϕ, deg	θ, deg	θ–ϕ, deg
0.20	32.2	35.2	3	46.9	48.3	1.4	25.7	47	21.3
0.35	46.9	48.7	1.8	46.9	49	2.1	32.2	46.1	13.9
0.50	46.9	49.1	2.2	46.9	50.1	3.2	46.9	53.6	6.7
0.65	25.7	46.8	21.1	32.2	45.7	13.5	25.7	56.5	30.8
0.80	46.9	50.9	4	32.2	50.5	18.3	46.9	56	9.1

Injector models are made of stainless steel. Eighteen models were designed through assembling different parts; the schematic of an injector model is shown in Fig. 5. A map of the measuring area and position in the spray field is sketched in Fig. 6. Each photograph shot at the measuring point shows a projection of all the droplets in the measuring area, which is vertical to the axes of the injector. Figure 7 shows some continuous-spray images at one measuring point shot in 5/4500 s continuously.

A pressure sensor and flow meter are fixed to the pipe near the injector. When the valve of the pipe is open, the high-speed camera begins to work, saving these photographs into an image analysis PC during 1 s. The experiment is repeated with different injector models under every operation condition.

IV. Results and Discussion

A. Comparison of Theoretical and Experimental Results for the Swirl Injector

All of the spray-sheet cone angles for the swirl injector in the present experimental setup were calculated, and a comparison between the results of the calculation and the experiment is shown in Table 1. The spray-sheet cone angle decreases due to the increase in swirl-injector spout length, the effect of viscosity is much more evident due to the increase in swirl-injector spout length, viscosity reduces the liquid-vortex flow momentum, and the circular velocity of the liquid-swirl sheet will also decrease, which will decrease the spray-sheet cone angle. In addition, the spray sheet pulsates even

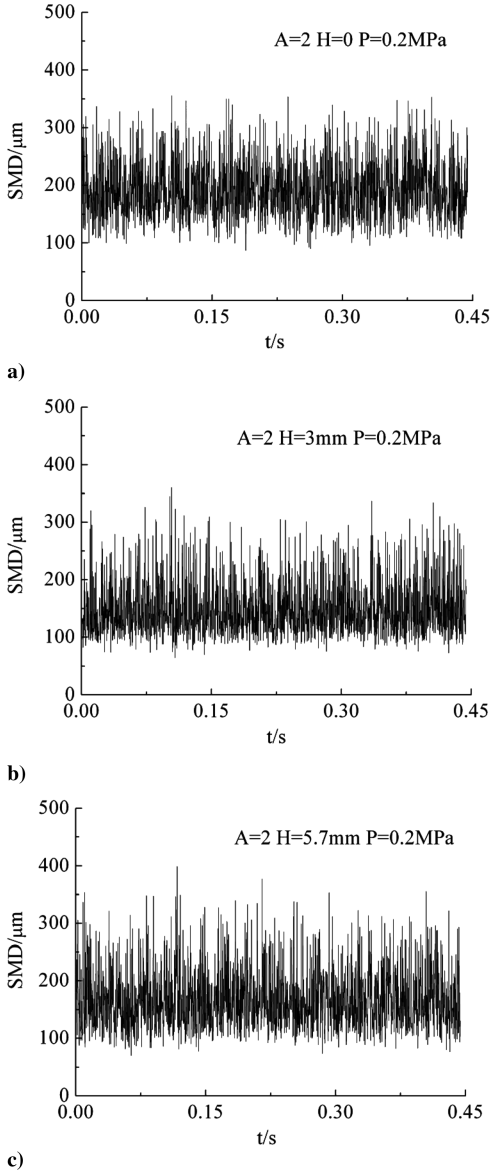

Fig. 8 Dependence of the SMD on time.

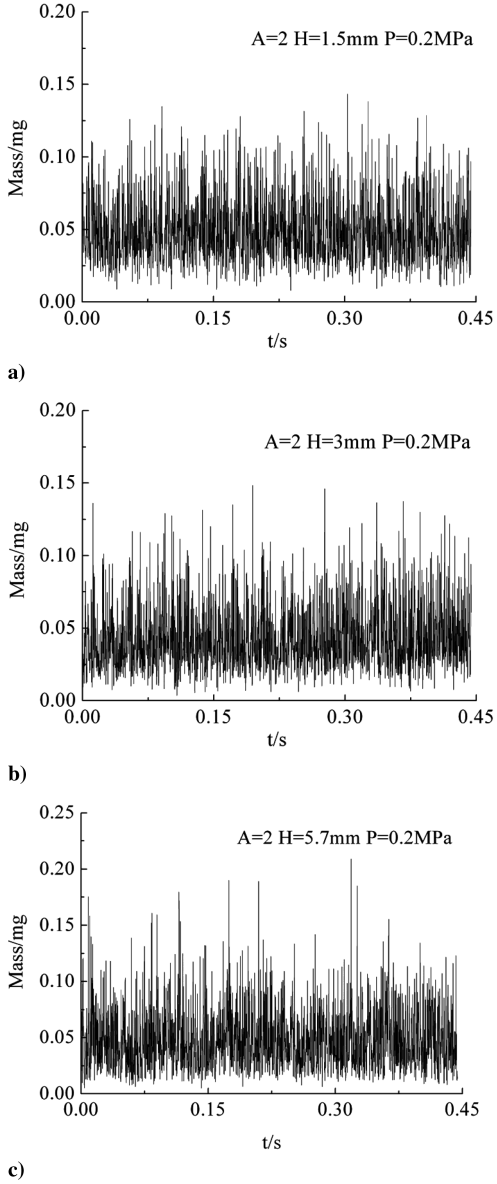

Fig. 9 Dependence of the droplet mass on time.

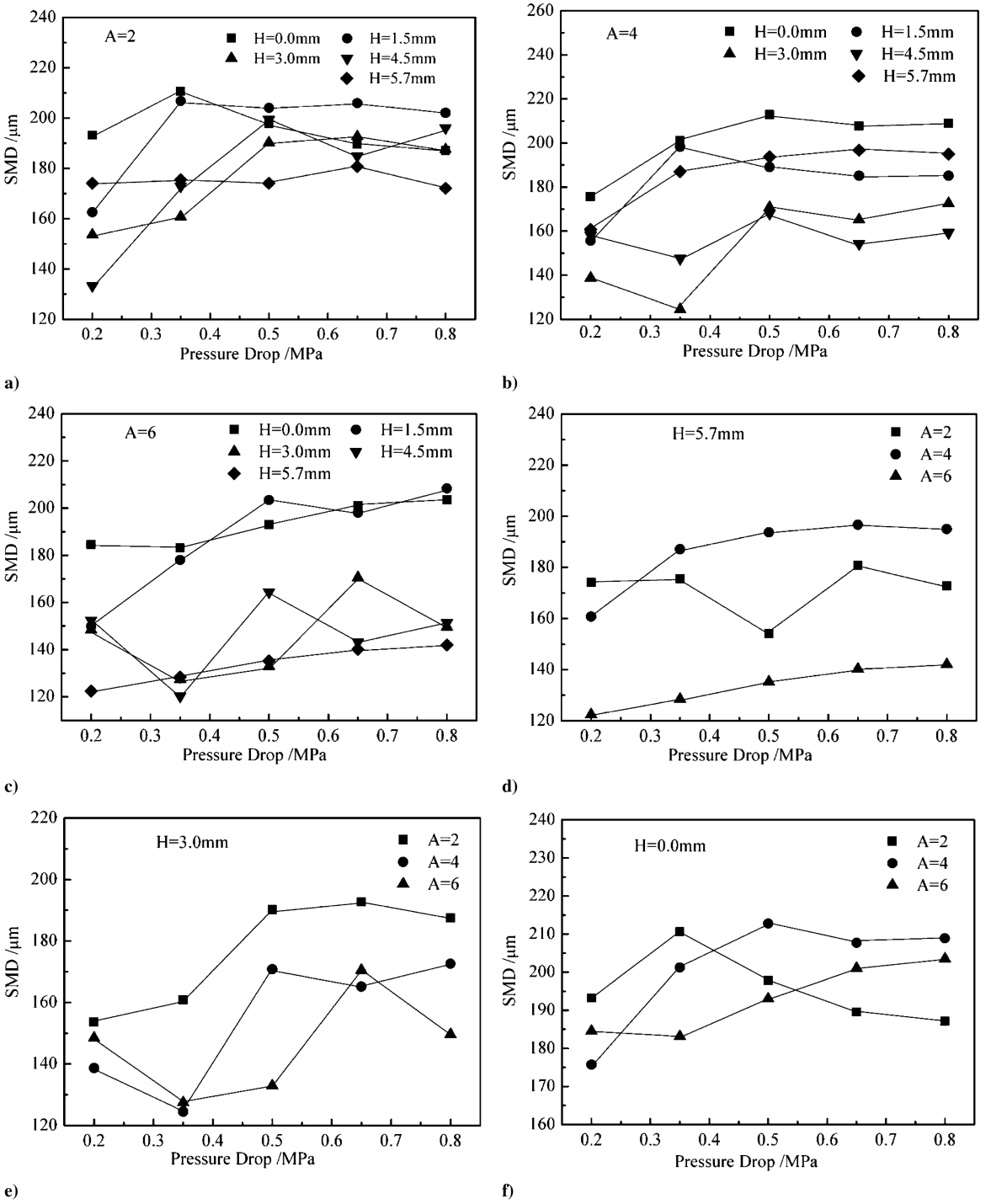

Fig. 10 Dependence of the SMD on ΔP.

under steady conditions. For the liquid-swirl center port of the coaxial injector in an ambient environment, photographs of atomization from the liquid-swirl center port are shown in Fig. 4.

The spray-sheet cone angle of the liquid-swirl center port will change with pressure drop, which is difficult to measure precisely. An approximate measurement can, however, be corrected based on theory. Suppose that

$$tg\frac{\theta_{\text{real}}}{2} = \alpha \cdot e^{\beta \cdot \frac{\Delta P}{P_0}} tg\frac{\theta_T}{2} \tag{4}$$

From the data shown in Table 1, according to the numerical calculation, α and β can be defined as $\alpha = 0.856$ and $\beta = 0.006$. For the swirl injector, an experiential expression can be obtained:

$$tg\frac{\theta_{\text{real}}}{2} = 0.856 \cdot e^{0.006 \cdot \frac{\Delta P}{P_0}} tg\frac{\theta_T}{2} \tag{5}$$

B. Change of Sauter Mean Diameter with Time in the Test Area

The image analysis system can calculate the Sauter mean diameter (SMD) in every photograph, and the high-speed camera can shoot 4500 photographs in 1 s. Therefore, a high-speed dynamic test system can calculate the SMD of droplets in the measuring area every 1/4500 s.

Through analysis of liquid droplets for each photograph under different operation conditions, the curve of Figs. 8a–8c show that the SMD is dependent on time in the measurement area of the different

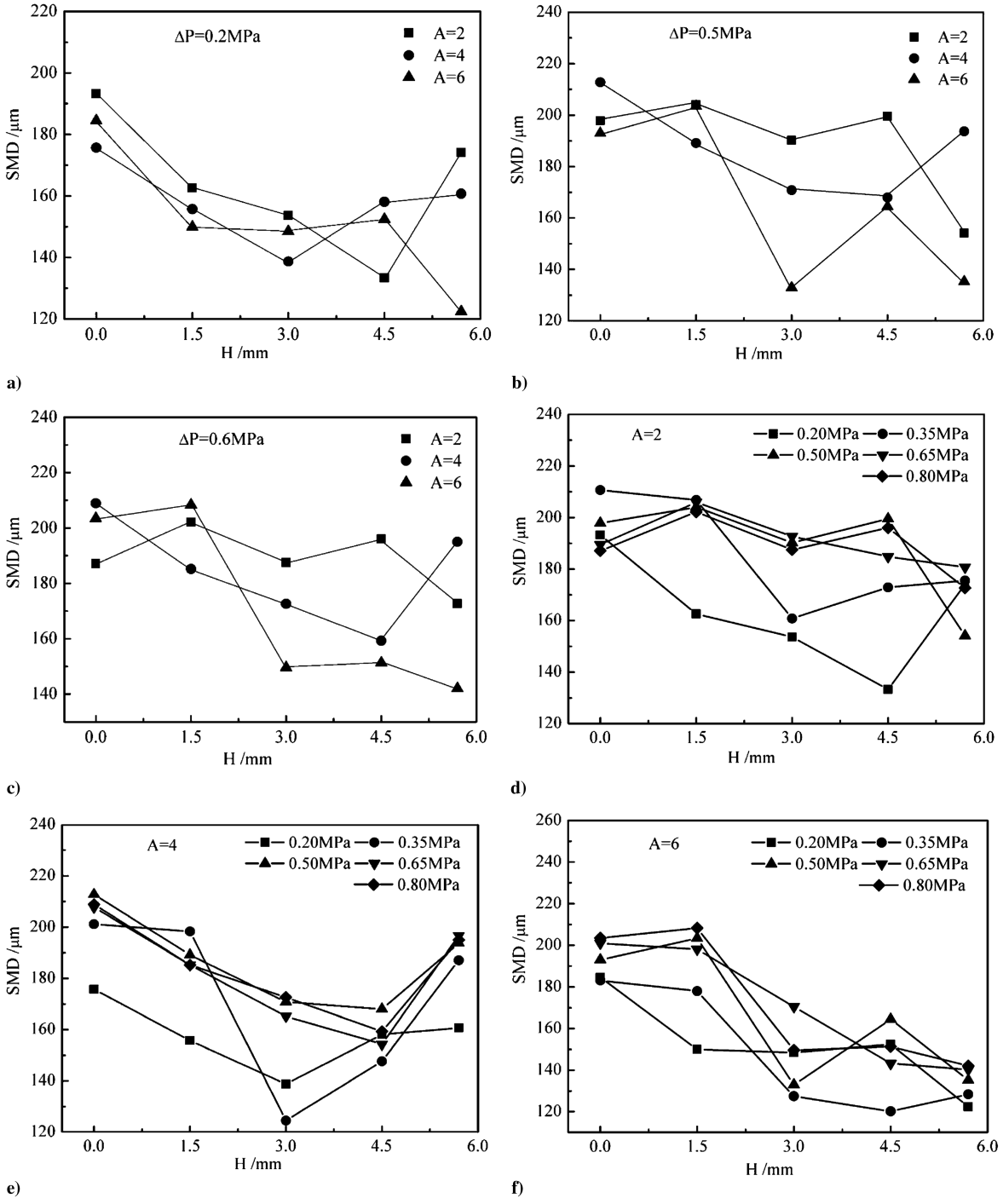

Fig. 11 Dependence of the SMD on recess length.

recess. These curves show that the atomization process of the coaxial injector is unsteady. In the measurement area of 2×2 mm^2, the SMD is variable, which results in variations in vaporization, mixing, and heat release in the combustion chamber.

C. Mass of Liquid Droplets Dependent on Time in the Test Area

The curves in Fig. 9 show that under different conditions, the mass of liquid droplets varies with time in the testing area for different injector models. The variation in liquid-droplet mass will result in the variation in heat release in the combustion chamber.

D. Changes of the SMD with Liquid Pressure Drop in the Injector

According to the analysis of 2000 continuous liquid-droplet photographs, the curves of the SMD varying with pressure drop, geometric characteristics parameter, and recess length are shown in Figs. 10a–10c. The effects of increasing liquid mass flow rate on liquid atomization can be classified: with the increase of liquid pressure drop, the liquid film velocity at the end face of the coaxial injector results in a decrease in the SMD. The liquid mass flow rate will vary with the liquid pressure drop. Because the gas-pressure drop and mass flow rate are fixed in the experiment, the amount of liquid that needs to be atomized will increase, and the SMD will also increase. In conclusion, with the increase in liquid pressure drop, the variation tendency of the SMD will depend on the preceding two factors. The specific atomization process is very complicated and depends on which of the preceding two factors dominates. When the geometric characteristic parameter A is equal to 2 and 4, liquid pressure drop is between 0.5 and 0.8 MPa, and the SMD of the liquid droplets gradually increases with pressure drop, perhaps because of

the equal effect of the two factors on the SMD. When the geometric characteristic parameter A is equal to 6, because of the evident centrifugal power, viscosity loss will increase, and the velocity at the swirl-injector end face will increase too, which will result in a variation of the SMD with the liquid pressure drop as a whole. The curves of the SMD varying with the pressure drop for different geometric characteristics and recess length are shown in Figs. 10d–10f.

E. Changes of the SMD with Swirl Center-Port Recess Length

The configuration of experimental coaxial injectors is shown in Table 2. Under different experimental conditions, the SMD varies with the recess length of different coaxial injectors, as shown in Fig. 11. When there is no recess or the recess length is low ($H = 0$ and 1.5 mm), the SMD is larger. For each experimental condition, there is one certain recess distance corresponding to the minimum value of the SMD. This experimental phenomenon can now be analyzed according to the preceding three proposed spray models. Under each experimental condition, a certain recess length corresponds to a minimum SMD. Differences between the recess angle of the coaxial injector and the swirl liquid spray-sheet cone angle were investigated, as shown in Table 3.

According to Table 3, spray-sheet cone angles are larger than the recess angles, possibly because the swirling liquid film collides on the inner surface of the outer gas-flow passage. This flow condition is the gas–liquid inner mixing flow. The difference between spray-sheet cone angle and the recess angle is no more than 10 deg for 9 of 15 testing points, considering the effects of measurement tolerances for the swirl liquid spray-sheet cone angle and influence of concentric gas flow. In fact, if the swirling liquid spray-sheet cone angle is no less than the recess angle (namely, $\phi \geq \theta$), the inner swirl liquid film sweeps the exit rim of the outer gas injector and produces a gas–liquid critical recess condition. For the other 6 test points, the difference between the swirl liquid spray-sheet cone angle and the recess angle is large (namely, $\phi < \theta$), which belongs to the gas–liquid inner mixing flow. For all the test positions, when the spray-sheet cone angle of the swirl injector is equal to or somewhat exceeds the recess angle, the SMD is small. For inner mixing flows, in which the spray-sheet cone angle of the swirl injector exceeds the recess angle, the SMD varies greatly. That is, when the inner swirl liquid film collides on the inner surface of the outer gas injector, the effects on atomization are more complex and difficult to analyze. According to the investigation, the three models of the recessed mixing chamber proposed are verified through experiments. For gas–liquid critical recess flows, the SMD is lower, whereas for gas–liquid outer mixing flows, the SMD is larger; for gas–liquid inner mixing flows, the variation of the SMD is complex.

According to this analysis, the optimal value of recess distance H_{SMD} can be deduced. Substituting $\phi = \theta$ in Eq. (1) and considering Eq. (5), the following expression can be deduced:

$$H_{\mathrm{SMD}} = (d_g - d_c) \Big/ \left(1.711 e^{0.006 \frac{\Delta P}{P_0}} \frac{2\mu_T A_T}{\sqrt{(1+S)^2 - 4\mu_T^2 A_T^2}} \right) \quad (6)$$

V. Conclusions

The concentric-orifice coaxial injector has become the preferred design on most cryogenic propellant applications. Typically, the liquid oxygen port is recessed from the injector face to improve the combustion stability. The effect of recess distance on spray characteristics was investigated in this paper. A high-speed dynamic testing system is employed to shoot the spray field and calculate the SMD of every moment at the measuring point. The results show that the spray field of the coaxial injector is unsteady and the sizes of the liquid droplets and the mass flow rate in the spray field are variable.

Theoretical analysis shows that the recessed mixing-chamber flows can be classified to three flow models *namely, outer mixing flows, critical mixing flows, and inner mixing flows) according to the recess length of the swirl liquid center port, which should be investigated for each special flowing characteristic. For the coaxial swirl injector, when the spray-sheet cone angle is equal to or slightly larger than the recess angle (namely, in the condition of critical mixing flow), the minimum SMD is produced.

Acknowledgment

This work was supported by the National Natural Science Foundation of China, project 50406007.

References

[1] Yang, V., and Anderson, W. E., *Liquid Rocket Combustion Instability*, Science Press, Beijing, 2001.

[2] Wanhainen, J. P., Parish, H. C., and Conrad, E. W., "Effect of Propellant Injection Velocity on Screech in 20000-Pound Hydrogen-Oxygen Rocket Engine," NASA TN D-3373, Apr. 1966.

[3] Burick, R. J., "Atomization and Mixing Gas/Liquid Coaxial Injectors," *Journal of Spacecraft and Rockets*, Vol. 9, No. 5, 1972, pp. 326–331. doi:10.2514/3.61681

[4] Sankar, S. V., Brena de la Rosa, A., Isakovic, A., and Bachalo, W. D., "Liquid Atomization by Coaxial Rocket Injectors," AIAA Paper 91-0691, Jan. 1991.

[5] Sasaki, M., Sakamoto, H., Takahashi, M., and Tamura, H., "Comparative Study of Recessed and Non-Recessed Swirl Coaxial Injector," AIAA Paper 97-2907, 1997.

[6] Hannum, N. P., Russell, L. M., Vincent, D. W., and Conrad, E. W., "Some Injector Element Detail Effects on Screech in Hydrogen-Oxygen Rockets," NASA TM X-2982, Feb. 1974.

[7] Sankar, S. V., Wang, G., Brena de la Rosa, A., Rudoff, R. C., Isakovic, A., and Bachalo, W. D., "Characterization of Coaxial Rocket Injector Sprays Under High Pressure Environments," AIAA Paper 92-0228, Jan. 1992.

[8] Falk, A. Y., "Coaxial Spray Atomization in Accelerating Gas Stream," NASA CR-134825, June 1975.

[9] Gomi, H., "Pneumatic Atomisation with Coaxial Injectors: Measurements of Drop Sizes by the Diffraction Method and Liquid Phase Fraction by the Attenuation of Light," National Aerospace Lab., NAL-TR-888T, Tokyo, Nov. 1985.

[10] Glogowski, M., and Micci, M. M., "Shear Coaxial Injector Spray Characterization Near the LOX Post Tip Region," 31st AIAA/ASME/SAE/ASEE Joint Propulsion Conference and Exhibit, AIAA Paper 95-2552, San Diego, CA, July 1995.

[11] Glogowski, M., Bar-Gill, M., Puissant, C., Kaltz, T., Milicic, M., and Micci, M., "Shear Coaxial Injector Instability Mechanisms," AIAA Paper 94-2774, 1994.

[12] Bazarov, V., "Self-Pulsations in Coaxial Injectors with Central Swirl Stage," AIAA Paper 95-2358, 1995.

[13] Kim, B., and Heister, S., "Two-Phase Modeling of Hydrodynamic Instabilities in Coaxial Injectors," *Journal of Propulsion and Power*, Vol. 20, No. 3, 2004, pp. 468–479. doi:10.2514/1.10378

[14] Yang, L., Ge, M., and Zhang, X., "Effects of Spout Length on Spray Characteristics of the Swirl Injector," *Journal of Propulsion Technology*, Vol. 26, No. 3, 2005, pp. 209–214.

V. Yang
Editor-in-Chief